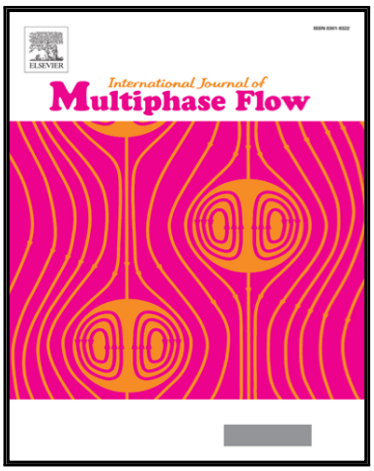

A new coupled level set and volume-of-fluid method to capture free surface on an overset grid system

Yucheng Zhao , Hamn-Ching Chen

PII: S0301-9322(16)30297-X
DOI: 10.1016/j.ijmultiphaseflow.2017.01.002
Reference: IJMF 2522

To appear in: *International Journal of Multiphase Flow*

Received date: 17 May 2016
Revised date: 8 January 2017
Accepted date: 15 January 2017

Please cite this article as: Yucheng Zhao , Hamn-Ching Chen , A new coupled level set and volume-of-fluid method to capture free surface on an overset grid system, *International Journal of Multiphase Flow* (2017), doi: 10.1016/j.ijmultiphaseflow.2017.01.002

Highlights

- A new coupled Level-Set and Volume-of-Fluid (CLSVOF) method is developed on an overset grid system.
- The CLSVOF method can capture accurate free surface.
- The CLSVOF method can preserve good local and stable mass conservation.

A new coupled level set and volume-of-fluid method to capture free surface on an overset grid system

Yucheng Zhao[a] and Hamn-Ching Chen[a]

[a] Department of Ocean Engineering, Texas A&M University, College Station, TX 77843-3136 USA

ABSTRACT

We present a new coupled level set and volume-of-fluid (CLSVOF) method for free surface flow simulations on an overset grid system. The coupled method takes advantages of the strengths of the level set (LS) method and the volume-of-fluid (VOF) method, and is superior to either single method. The novelty of the present method lies in that we develop the methodology for an overset grid system of embedding, overlapping and moving structured grids. The new methodology accurately captures interface and greatly preserves mass on an overset grid system by demonstrating the 3D sphere advection test. The method is coupled to a well validated Reynolds-Averaged Navier-Stokes incompressible flow solver. The method is validated with the dam-breaking flow interacting with a 3D obstacle (square structure/circular cylinder) by comparing the numerical results with available experimental and numerical studies. The water impact of a sphere case is further performed to demonstrate the capabilities of the new method on a complicated moving overset grid system.

1. Introduction

The numerical simulation of flows involving two different immiscible fluids with a well-defined interface is a very common topic in a variety of industrial processes and natural phenomena. It is a considerable challenge for the numerical prediction of immiscible two-phase flow simulation because the interface must be tracked or predicted simultaneously with the flow field evolution. In particular, accurate representation and advection of the interface is essential for the numerical simulation. Extensive studies have been devoted to the prediction of two-phase fluids flow over the past several decades [1-5].

The volume-of-fluid (VOF) method and the level set (LS) method are the most popular numerical strategies to predict interface motion among several interface-capturing methods. Hirt and Nichols [2] proposed the volume-of-fluid (VOF) method to track the free surface. The interface is represented by the VOF function which denotes the volume fraction occupied by one fluid in each cell. The VOF function's value is between zero and one in cells cut by the interface.

The values are zero or one where the cells are away from the interface. When the value of the VOF function is outside the range of the consistency property, it indicates that the law of physics is violated. Particular attention must be given to avoid introducing too much numerical diffusion while maintaining the shape interface. In general, interface reconstruction and interface advection are the two essential procedures in the VOF method. Interface reconstruction is used to evaluate an approximation to the section of the interface in each cut cell. The interface reconstruction has been derived from the original simple line interface calculation (SLIC) [6] to piecewise linear interface construction (PLIC) [7]. Once the interface has been reconstructed, its motion must be modeled by a suitable interface advection algorithm. Most of the interface advection algorithms are based on structured grids, either with a split scheme [8-10] or an un-split scheme [8, 11]. Although the VOF method has a good mass conservation property, it suffers from the challenge of accurately calculating interface normal and curvature due to that the VOF function is discontinuous. Several algorithms have been developed for normal vector calculations, most of them are less than second order accurate. Curvature calculations are even more difficult because they involve taking second order of the VOF function. It is worthwhile to note that the height-function (HF) method has been used to improve the accuracy of the curvature calculations [12-14]. The HF method is also substantially simpler to implement than other high-order methods. Another interface capturing method is the level set method [3]. The interface is captured by a level set function. The level set function is a smooth function and is initialized as the signed distance from the interface. The value is zero on an interface, negative in one phase, and positive in the other phase. The level set method is able to handle the complex interface geometry automatically, and it is not necessary to explicitly reconstruct the interface as the VOF method does. Since the level set function is a smooth function, the interface normal and

curvature can be accurately calculated from the level set function. The drawback is that the level set method is not able to preserve mass conservation because of the numerical dissipation across the interface. It is prone to more numerical error when the interface experiences severe stretching or tearing. Several algorithms about using high-order discretization of the level set equation [15, 16] and the new level set re-initialization [17-19] have been developed, but mass conservation is still an issue for simulations.

Taking advantages of mass conservation property of the VOF method and high-accuracy interface geometry calculation of the level set method, a coupled level set and VOF method (CLSVOF) has been developed by Sussman et al. [20, 21]. Since that, several variants of the CLSVOF method have been applied in various applications for structured grids [22, 23]. In addition, some works about the CLSVOF method have been presented on unstructured grids [24, 25]. Sussman et al. have also developed a CLSVOF method for an adaptive Cartesian grid [26]. However, most of the previous works about the CLSVOF method are applied to a single grid. The implementation of the CLSVOF method on an overset grid system is not covered. The overset grid approach with the CLSVOF method provides an elegant solution to the problems involving the free surface flow around moving bodies, or bodies with very complex geometries. In these scenarios, it is promising to use overset grid system for the free surface flow simulations. The immersed boundary method [27] is another attractive method to handle arbitrarily complex geometries and/or moving bodies. The advantage of this approach is that the mesh does not need to conform to the obstacles, reducing the mesh generation effort. The limitation arises when applying an immersed boundary method to a flow problem involving moving bodies undergoing large displacement and/or complex multi-connected geometries. The overset grid approach allows us to handle arbitrary large amplitude body motions without tedious and costly grid-

regeneration. The complex flow domain is decomposed into a set of simple, overlapping subdomains such that it can be discretized easily with a set of simple, boundary conforming, curvilinear coordinates. The governing equations are solved independently on each subdomain and information from one subdomain is transferred to another subdomain by specifying the boundary conditions. Moreover, the boundary-fitted grids enable us to provide accurate and efficient resolution of turbulent boundary layers at very high Reynolds numbers.

In this study, we present a new CLSVOF method for free surface flow simulation on an overset grid system including embedding, overlapping and moving structured grids. The present work inherits the work about the level set Reynolds-Averaged Navier-Stokes (RANS) method for the predictions of various free surface problems [28]. In our work, we use a fifth-order weighted essentially non-oscillatory (WENO) scheme [29] for the evolution of the level set function. For the advection of the volume of fluid method, the PLIC method by Gueyffier et al. [30] is employed as the interface reconstruction algorithm while the interface advection algorithm is presented in the framework of a mixed split Eulerian implicit-Lagrangian explicit interface advection scheme by Scardovelli and Zaleski [10, 34]. Different from the works by Scardovelli and Zaleski, our interface advection scheme is using a mixed second-order Lagrangian and Eulerian scheme. In addition, a volume-correction scheme is developed to compensate for the mass change and to maintain a divergence-free velocity field. Moreover, a special scheme is performed for evaluation of the VOF function at each fringe grid point on an overset grid system. In our previous works, several numerical cases including sloshing flow case and wave slamming flow case were performed and validated [31, 32]. In this work, we performed several numerical cases to demonstrate that our framework is good at mass conserving and interface capturing on an overset system of multiple structured grids.

2. Governing equations

As mentioned in Section 1, the level set function, specified as ϕ, is the signed distance from the interface. The region of each phase can be distinguished by the sign of the level set function.

$$\phi(\vec{x},t)\begin{cases} >0 & \textit{fluid A} \\ =0 & \textit{interface} \\ <0 & \textit{fluid B} \end{cases} \tag{1}$$

The VOF function, defined as C, represents the volume fraction of the fluid in a computational cell. The value of the VOF function in every cell denotes a volume fraction occupied by one fluid

$$C(\vec{x},t)\begin{cases} =1 & \textit{fluid A} \\ \in]0;1[& \textit{interface} \\ =0 & \textit{fluid B} \end{cases} \tag{2}$$

The advection equations of the level set function and VOF function during time t with the underlying velocity $\vec{V}$ are written as follows

$$\frac{\partial \phi}{\partial t} + \vec{V} \cdot \nabla \phi = 0 \tag{3}$$

$$\frac{\partial C}{\partial t} + \vec{V} \cdot \nabla C = 0 \tag{4}$$

The geometric properties, such as interface normal $\vec{m}$ and curvature κ are presented as,

$$\begin{cases} \vec{m} = \dfrac{\nabla \phi}{|\nabla \phi|} \\ \kappa = \nabla \cdot \dfrac{\nabla \phi}{|\nabla \phi|} \end{cases} \tag{5}$$

In this study, the continuum surface force (CSF) method was used to smooth the fluid properties across the interface. More specifically, the fluid properties, such as density ρ and dynamic

viscosity μ, depend on the level set function. The region where both the density and the viscosity vary is defined as a transition zone. The transition zone is defined by $|\phi| \le \varepsilon$, where ε is half the thickness of the interface. In the transition of the interface, non-dimensional density $\rho(\phi)$ and non-dimensional dynamic viscosity $\mu(\phi)$ can be smoothed by the smoothed Heaviside function.

$$\begin{cases} \rho(\phi) = \rho_B / \rho_A + (1 - \rho_B / \rho_A) \times H(\phi) \\ \mu(\phi) = \mu_B / \mu_A + (1 - \mu_B / \mu_A) \times H(\phi) \end{cases} \text{ (Normalized by fluid } A, C = 1) \tag{6}$$

The smoothed Heaviside function is specified as,

$$H(\phi) = \begin{cases} 0 & if\ \phi < -\varepsilon \\ \frac{1}{2}\left(1 + \frac{\phi}{\varepsilon} + \frac{1}{\pi}\sin(\frac{\pi\phi}{\varepsilon})\right) & if\ -\varepsilon \le \phi \le \varepsilon \\ 1 & if\ \phi > \varepsilon \end{cases} \tag{7}$$

By normalization of characteristic length L, characteristic velocity U_0 and characteristic time $T_0 = L / U_0$, the two-phase flow is governed by the conservation of momentum and the conservation of mass in the following dimensionless forms,

$$\begin{cases} \rho(\phi)\left(\frac{\partial \vec{V}}{\partial t} + \vec{V} \cdot \nabla \vec{V}\right) = -\nabla\left(p + \frac{\rho(\phi) z}{Fr^2}\right) + \frac{1}{\mathrm{Re}} \nabla \cdot \left(\mu(\phi)\left(\nabla \vec{V} + (\nabla \vec{V})^T\right)\right) \\ \nabla \cdot \vec{V} = 0 \end{cases} \tag{8}$$

where z is the normalized Cartesian coordinate in vertical direction, p is the non-dimensional pressure and $\vec{V}$ is non-dimensional the velocity. Froude number is $Fr = \sqrt{\frac{U_0^2}{gL}}$ and Reynolds number is $\mathrm{Re} = \frac{\rho_A U_0 L}{\mu_A}$.

3. CLSVOF method

According to the principle of the CLSVOF method, the interface is captured by the level set function, which is corrected to ensure mass conservation under the framework of the VOF

function. The geometrical properties of the interface are described by the level set function. The level set function is re-distanced by the VOF function.

The level set advection equation (Eq. (3)) and the VOF advection equation (Eq. (4) can be transformed from the Cartesian coordinates $x^i = (x, y, z)$ to the general curvilinear coordinates $\xi^i = (\xi, \eta, \zeta)$ as following

$$\frac{\partial \phi}{\partial t} + U\frac{\partial \phi}{\partial \xi} + V\frac{\partial \phi}{\partial \eta} + W\frac{\partial \phi}{\partial \zeta} = 0 \tag{9}$$

$$\frac{\partial (JC)}{\partial t} + (JU)\frac{\partial C}{\partial \xi} + (JV)\frac{\partial C}{\partial \eta} + (JW)\frac{\partial C}{\partial \zeta} = 0 \tag{10}$$

$U^i = (U, V, W)$ are the contravariant velocity components in the transformed grid and defined by Eq.(11). J is the Jacobian transformation which represents the physical volume for each computational cell.

$$U^i = \xi^i_{,x}u + \xi^i_{,y}v + \xi^i_{,z}w \tag{11}$$

3.1 Interface reconstruction

The key part of the interface reconstruction is to determine the orientation of the interface segments in every surface cell. An explicit expression by Gueyffier et al. [30] is employed. For 3D cases, the interface in the transformed grid is represented by a 3D plane as follows

$$m_1\xi + m_2\eta + m_3\zeta = \alpha \tag{12}$$

where α is a parameter which indicates the shortest distance from the origin to the 3D plane. The interface normal vector $\vec{m} = (m_1, m_2, m_3)$ can be obtained from the level set function by Eq. (5).

On the one hand, the "forward" problem is to find the cut volume, *VL*, under certain interface orientation within the cell spacing (c_1, c_2, c_3). The expressions are given below in three different forms (Eq. (13) - (15)),

When all the components of interface normal $\vec{m} = (m_1, m_2, m_3)$ are nonzero, the expression of the 3D volume is,

$$VL = \frac{1}{6|m_1 m_2 m_3|}[\alpha^3 - \sum_{j=1}^{3} H(\alpha - |m_j|c_j)(\alpha - |m_j|c_j)^3 + \sum_{j=1}^{3} H(\alpha - \alpha_{MAX} + |m_j|c_j)(\alpha - \alpha_{MAX} + |m_j|c_j)^3] \quad (13)$$

where $\alpha_{MAX} = |m_1|c_1 + |m_2|c_2 + |m_3|c_3$, and $H(x) = \begin{cases} 0 & for\ x < 0 \\ 1 & for\ x > 0 \end{cases}$.

When only one component of interface normal $\vec{m} = (m_1, m_2, m_3)$ is zero, the expression of the volume is reduced to the 2D area multiplied by the interface "thickness",

$$VL = \frac{1}{2|m_1 m_2|}[\alpha^2 - \sum_{j=1}^{2} H(\alpha - |m_j|c_j)(\alpha - |m_j|c_j)^2] \times c_3 \qquad (Case: m_3 = 0) \quad (14)$$

When only one component of interface normal is nonzero, the volume is straightforward to compute volume of a cube,

$$VL = \alpha \times c_1 \times c_2 \qquad (Case: m_3 \neq 0) \quad (15)$$

On the other hand, because the relation between *VL* and α is one-to-one, the "inverse" problem of determining the parameter α given a cut volume and normal direction $\vec{m} = (m_1, m_2, m_3)$ in a computational cell can be solved using a standard root-finding approach. In this study, the Brent's method [33] is employed to find the polynomial root. In general, both the "forward" and "inverse" problems are needed in the reconstruction step and the following steps.

3.2 Interface advection

A mixed split Eulerian implicit-Lagrangian explicit (EI-LE scheme) was presented by Scardovelli and Zaleski, which can conserve the mass to machine error under the discrete divergence-free velocity field [10, 34]. The mixed scheme is decomposed into an Eulerian implicit scheme in one direction followed by a Lagrangian explicit step in the other one. The

Lagrangian scheme was presented in detail by Gueyffier et al. [30]. Wang et al. used a second-order Runge-Kutta scheme for time integration by using Gueyffier's Lagrangian advection scheme and showed the improvement in the results [23]. The Eulerian scheme was introduced by Rider and Kothe [8]. In our study, we extend the EI-LE scheme to the transformed plane and also employ a second-order Runge-Kutta scheme in the EI-LE scheme [35, 36].

A mixed EI-LE scheme for a 2D case is to combine an Eulerian step along one direction followed by a Lagrangian step in the other direction on the basis of split technique to propagate the interface separately. Take the EI-LE scheme in the ξ–ζ plane as an example. During one-time step from t^n to t^{n+1}, the interface within the cell (i, j, k) is firstly propagating along ξ direction by the Eulerian-implicit (EI) scheme in Fig. 1(a). The intermediate VOF function, C^*_{ijk}, is obtained after 1D advection along ξ direction

$$C^*_{ijk} = \frac{J_{ijk} C^n_{ijk} + VL_{L,ijk} / (\Delta\xi\Delta\eta\Delta\zeta)_{ijk} - VL_{R,ijk} / (\Delta\xi\Delta\eta\Delta\zeta)_{ijk}}{J_{ijk}(1 + Dis_{L,ijk} / \Delta\xi_{ijk} - Dis_{R,ijk} / \Delta\xi_{ijk})} \tag{16}$$

where VL_L and VL_R represent the volume of one phase fluid across the left and the right faces, respectively. U_R and U_L are the velocities on the left and the right faces. Dis_L and Dis_R are the travelling distances for the liquid through left and right faces during the time increment $\Delta t = t^n - t^{n-1}$. The travelling distances in Eq. (17) are evaluated by using a second-order Runge-Kutta method.

$$\begin{cases} Dis_L = U_L \Delta t - 0.5 U_L \Delta t^2 A \\ Dis_R = U_R \Delta t - 0.5 U_R \Delta t^2 A \end{cases}; \quad A = \frac{U_R - U_L}{\Delta\xi} \tag{17}$$

The volume in the cell (i, j, k) is VL^*_{ijk} in Eq. (18),

$$VL^{*}_{ijk} = J_{ijk}(\Delta\xi\Delta\eta\Delta\zeta)_{ijk} \times C^{*}_{ijk} = \frac{J_{ijk}(\Delta\xi\Delta\eta\Delta\zeta)_{ijk} C^{n}_{ijk} + VL_{L,ijk} - VL_{R,ijk}}{1 + Dis_{L,ijk}/\Delta\xi_{ijk} - Dis_{R,ijk}/\Delta\xi_{ijk}} \tag{18}$$

After propagating in the ξ direction by the Eulerian-implicit scheme, the VOF function is updated to an intermediate level. The interface normal is updated by the intermediate level set function by the similar split advection scheme. Another interface reconstruction procedure is carried out to obtain the new orientation of the interface in the cell (Fig. 1(b)). The following step is the advection along the ξ direction by the Lagrangian-explicit (LE) scheme. The detailed procedure for the propagation of the interface by the velocities is presented by Gueyffier et al. [30]. After the Lagrangian advection, the interface might protrude into the neighboring cells. Similarly, the interface which belongs to the neighboring cells might also enter the present cell. The portion of the liquid volume that remains in the original cell are defined as VL_O; the liquid volumes from top and bottom neighboring cells to enter the current cell are defined as VL_T, VL_B, shown in Fig. 1(c). The VOF function after one application of the EI-LE scheme in ξ–ζ plane is C^{**}_{ijk},

$$C^{**}_{ijk} = \frac{VL_{O,ijk} + VL_{B,ijk} + VL_{T,ijk}}{J_{ijk}(\Delta\xi\Delta\eta\Delta\zeta)_{ijk}} \tag{19}$$

Similar with Eq. (17), the corresponding distances Dis_T and Dis_B for top and bottom faces in Fig. 1(c) can be updated by using a second-order Runge-Kutta method in $\Delta t = t^{n+1} - t^{n}$,

$$\begin{cases} Dis_B = W_B\Delta t + 0.5W_B\Delta t^2 B \\ Dis_T = W_T\Delta t + 0.5W_T\Delta t^2 B \end{cases};\ B = \frac{W_T - W_B}{\Delta\zeta} \tag{20}$$

where W_B and W_T are the velocities on the bottom and the top faces.

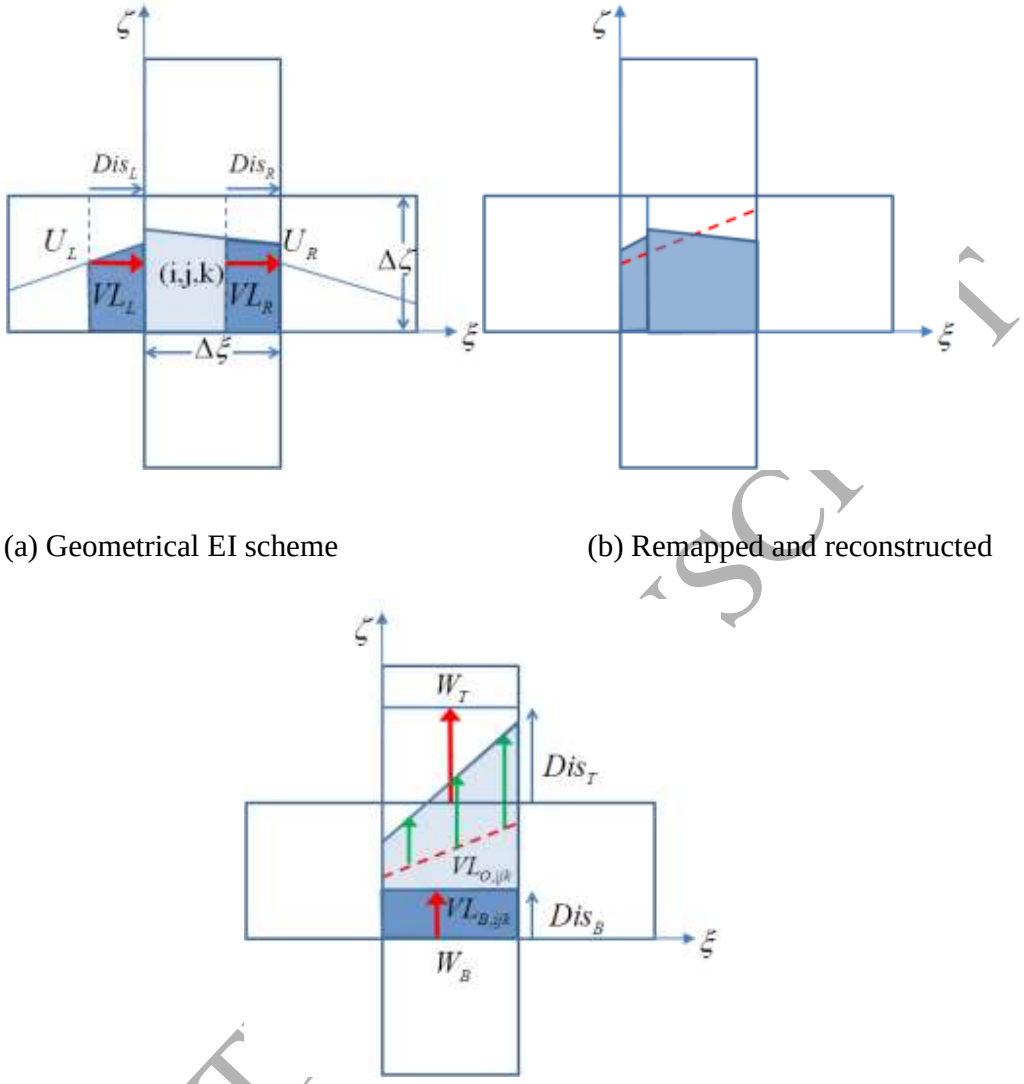

(a) Geometrical EI scheme (b) Remapped and reconstructed

(c) Geometrical LE scheme

Fig. 1. 2D EI-LE interface advection scheme

The 2D EI-LE scheme can preserve the exact volume conservation under the divergence-free velocity (Eq. (21)).

$$\frac{(U_{R,ijk}-U_{L,ijk})}{\Delta\xi_{ijk}}+\frac{(W_{T,ijk}-W_{B,ijk})}{\Delta\zeta_{ijk}}=0 \tag{21}$$

The total volume can be proved as mass-conserving after one application of the EI-LE scheme analytically in our previous works [35, 36]. However, the velocity obtained from the numerical flow solver may not be able to achieve exact discrete divergence-free condition. For instance, the flow solver adopts the variable density and viscosity (Eq. (6)) in the interface transition zone. It indicates the velocity cannot be divergence-free condition in the transition region. To preserve exact mass conservation, we introduce an extra term $\varepsilon \times VL^*_{ijk}$ to maintain the mass conservation, where

$$\varepsilon = Dis_{B,ijk} / \Delta\zeta_{ijk} - Dis_{T,ijk} / \Delta\zeta_{ijk} + Dis_{L,ijk} / \Delta\xi_{ijk} - Dis_{R,ijk} / \Delta\xi_{ijk} \tag{22}$$

The volume-correction term $\varepsilon \times VL^*_{ijk}$ exists in every cell within the domain. The summation of the volume-correction over the domain can be collected and redistributed to the interface cells in the domain. More precisely, the domain can be divided into pieces of region; every region has its own volume-correction summation which is only redistributed to the interface cells within its domain.

For 3D EI-LE scheme, the velocity field (U,V,W) is decomposed into three sub-velocity fields: $(U_1,V_1,0)$, $(0,V_2,W_1)$, and $(U_2,0,W_2)$. It is required that each sub-velocity field is discrete divergence free as Eq. (21) if the original EI-LE scheme is used. Aulisa et al. proposed a EILE-3D scheme to do such decomposition [34]. However, a critical problem for EILE-3D scheme is that each sub velocity field cannot satisfy the boundary condition, although the sum of them can. In other words, the sub velocity fields can generate a back and forth motion on the boundary. By introducing the volume-correction term in our method, the three new 3D sub-velocity fields are not required to be incompressible. Generally, the velocity field can be divided equally into $(0.5U,0.5V,0)$, $(0,0.5V,0.5W)$, and $(0.5U,0,0.5W)$. Each velocity field does satisfy the

boundary condition. After going through EI-LE scheme under the three velocity fields above, the VOF function is fully updated to new time level. It is desirable to alternate the sequence of the three velocity fields to remove possible asymmetries.

3.3 LS re-distance

In the CLSVOF method, the coupling between the LS function and the VOF function occurs when computing the interface properties and also when adjusting the LS function with the exact signed distance to the reconstructed interface. The LS function must be adjusted by the reconstructed interface for mass conservation. Many researchers have proposed different re-distance algorithms [20, 37-40], which are mainly dealing with the 2D cases. Wang et al. proposed another new re-distance algorithm which can simplify the procedure and also can be extended to a general structured grid [23, 41]. In this study, the re-distance algorithm of Wang et al. in transformed grid [23] is adopted. Another straightforward scheme to transform the LS function from transformed grid to physical grid is used [42].

3.4 CLSVOF method on overset grid system

The present CLSVOF method is developed for overset grid system of embedding, overlapping, and moving grids for accurate resolution of complex geometries. The Chimera grid method [43, 44] is defined as the standard overset interpolation in our method. The standard overset interpolation technique has been used for the level set equation at each fringe point [28] because the level set function is smooth. However, it is invalid to interpolate the VOF function at fringe point since the volume fraction varies with the computational cell size. We update the VOF function at fringe point through the local level set function.

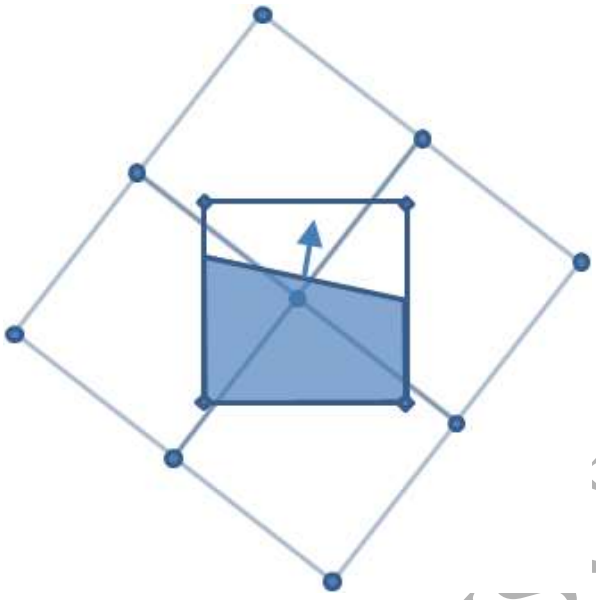

(a) Cell embedded in background grid

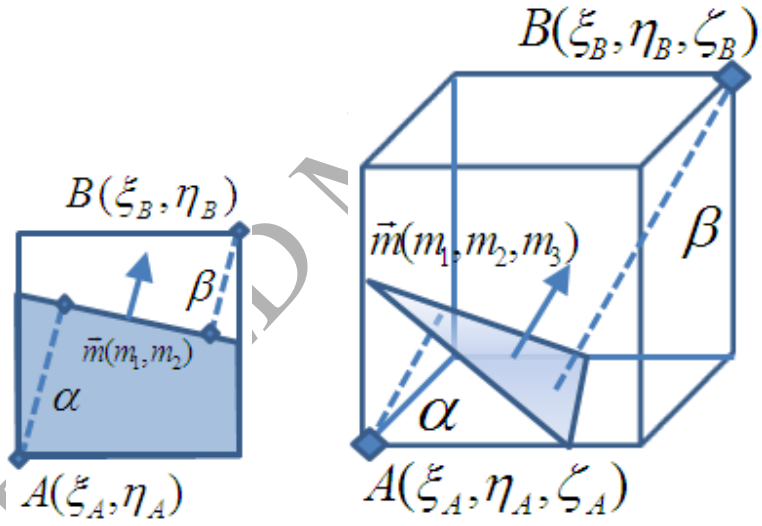

(b) 2D and 3D computational cell

Fig. 2. Evaluation of the VOF function at fringe point

In Fig. 2(a), one computational cell, which belongs to a fringe point of another grid, is embedded in background grid. The VOF of this cell is $C^{ijk}_{fringe-A}$ after one complete 3D EI-LE advection scheme. Firstly, the level set function at every corner point can be interpolated using the standard Chimera technique, for each cell at fringe point. The local origin is chosen as the

corner point with the largest level set function value. In Fig. 2(b), point *A*, $\vec{x}_A = (\xi_A, \eta_A, \zeta_A)$ is the local origin. The parameter α indicates the shortest distance from point *A* to the interface plane in Eq. (12). Similarly, β denotes the shortest distance from point *B*, which is opposite to point *A*. It is noted that the parameters α and β are the distances in the transformed grid; while the level set function at point *A* and point *B* are the physical distances. It is assumed that the ratios of the distances between point *A* and point *B* in the transformed and physical grids are identical,

$$\frac{\alpha}{\beta} = \left|\frac{\phi_A}{\phi_B}\right| \tag{23}$$

For the interface equation in this interface cell,

$$m_1\xi + m_2\eta + m_3\zeta = \alpha \tag{24}$$

The parameter β can be estimated by Eq. (24),

$$\left|m_1\xi_B + m_2\eta_B + m_3\zeta_B - \alpha\right| = \beta \tag{25}$$

Combining Eq. (23) and Eq. (25), the parameter α can be solved. The evaluation of the VOF function is turned into the "forward" problem in interface reconstruction algorithm (Eq. (13) - (15)). Once the "forward" problem is solved, the VOF of this cell becomes $C^{ijk}_{fringe-B}$, which is consistently coupled with the local LS functions.

In the section of the interface advection, it has been demonstrated that the EI-LE scheme with the volume-correction term can conserve the precise mass within a single domain. The present EI-LE scheme with the volume-correction term is employed for every grid block in overset grid system. It indicates that every grid block is able to conserve the mass conservation within its own domain. However, the inter-grid communication for the VOF function is required to pass the VOF function information from one grid to another. This technique is consistently related with the local LS function which does not possess the capability of mass conservation. To

maintain global mass conservation over the entire overset grid system, the additional volume-correction procedure has been incorporated into the present algorithm to enforce mass conservation on overset grid system.

For non-moving overset grid system, each grid block is fixed as well as all the fringe points, field points and hole points. The VOF function at any fringe point changed from $C^{ijk}_{fringe-A}$ to $C^{ijk}_{fringe-B}$ might lead to some mass variation. Thus, the VOF function change ($C^{ijk}_{fringe-A} - C^{ijk}_{fringe-B}$) should be calculated. For each fringe point, the VOF function change ($C^{ijk}_{fringe-A} - C^{ijk}_{fringe-B}$) can be accounted into the extra fluid amount into the fringe point's outer mesh. Therefore, the summation of the VOF function changes over all the fringe points need to be collected and redistributed to the interface cells over the entire overset grid system. For moving overset grid system, some of grid blocks may be moving in arbitrary manners. Thus, the point type (field point, fringe point and hole point) is not fixed all the time. The VOF function at certain point might also change the value once the point type is changed. Such changes of the VOF function value are also calculated and redistributed to the interface cells over the overset grid system as well.

4. Advection test on an overset grid system

One advection benchmark test case is performed to demonstrate the 3D interface capturing ability of the present CLSVOF method. This test case proposed by LeVeque [45] concerns with the stretching of a liquid sphere in a swirling shear velocity field. A number of interface tracking/capturing methods used this test case as a benchmark case [40, 41, 46]. In present work, the objective of this test case is to evaluate how well the EI-LE interface advection scheme conserves mass and handles the development of the stretched and deformed interface to a large extent on an overset grid system.

In this case, a 3D incompressible flow in a 1.0×1.0×1.0 dimensionless solution domain is prescribed by Eq. (26), with a dimensionless oscillation period T = 3.0 and the time increment of 0.5. A sphere with a radius of 0.15 is centered at (0.35, 0.35, 0.35).

$$\begin{cases} u = 2\sin^2(\pi x)\sin(2\pi y)\sin(2\pi z)\cos(\dfrac{\pi t}{T}) \\ v = -\sin(2\pi x)\sin^2(\pi y)\sin(2\pi z)\cos(\dfrac{\pi t}{T}) \\ w = -\sin(2\pi x)\sin(2\pi y)\sin^2(\pi z)\cos(\dfrac{\pi t}{T}) \end{cases} \tag{26}$$

Two relative errors are defined to quantify the conservation of mass during the surface advection. The relative mass error E_{mass} is,

$$E_{mass} = \frac{|\sum_{ijk} J_{ijk} C_{ijk} - \sum_{ijk} J_{ijk} C_{ijk,0}|}{\sum_{ijk} J_{ijk} C_{ijk,0}} \tag{27}$$

The relative geometry error $E_{geometry}$ is,

$$E_{geometry} = \frac{\sum_{ijk} J_{ijk} |C_{ijk} - C_{ijk,0}|}{\sum_{ijk} J_{ijk} C_{ijk,0}} \tag{28}$$

Firstly, the case is performed on a uniform Cartesian grid of 150×150×150. Fig. 3 shows the deformed shapes of the sphere at t = 1.5 and t = 3. The full velocity field combines a deformation in the x-y plane and another deformation in the x-z plane. Therefore, the sphere is stretched by these two rotating vortices to stretch out the middle part of the interface until t = 1.5 (Fig. 3(a)). And then, it goes on to return to the initial position at t = 3 (Fig. 3(b)). Wang et al. also presented the sphere deformation test on the same uniform Cartesian grid of 150×150×150 [23]. Their interface patterns are similar to our results in Fig. 3. In addition, it is clearly seen that our CLSVOF method can handle to resolve very thin interface in the middle of the stretched shape at t = 1.5, in Fig. 3(a). Only a small region of the shape is under-resolved. The occurrence

of this type of break-up is due to the fact that it is assumed there only exists one piecewise linear segment in the cut cell. When the interface filament is smaller than one grid spacing, one piecewise linear segment cannot fully describe the specific structure. It is notable that Menard et al. proposed the correction on the number of points in the stencil when two interface fronts are in the stencil domain [40]. The improved result is very remarkable in capturing the fine filaments. Furthermore, the present CLSVOF method is also able to maintain excellent mass conservation with a relative mass change of $1.32\times10^{-5}\%$, at the end of one period. In [23], the relative mass error is reported as 0.4% after one complete period.

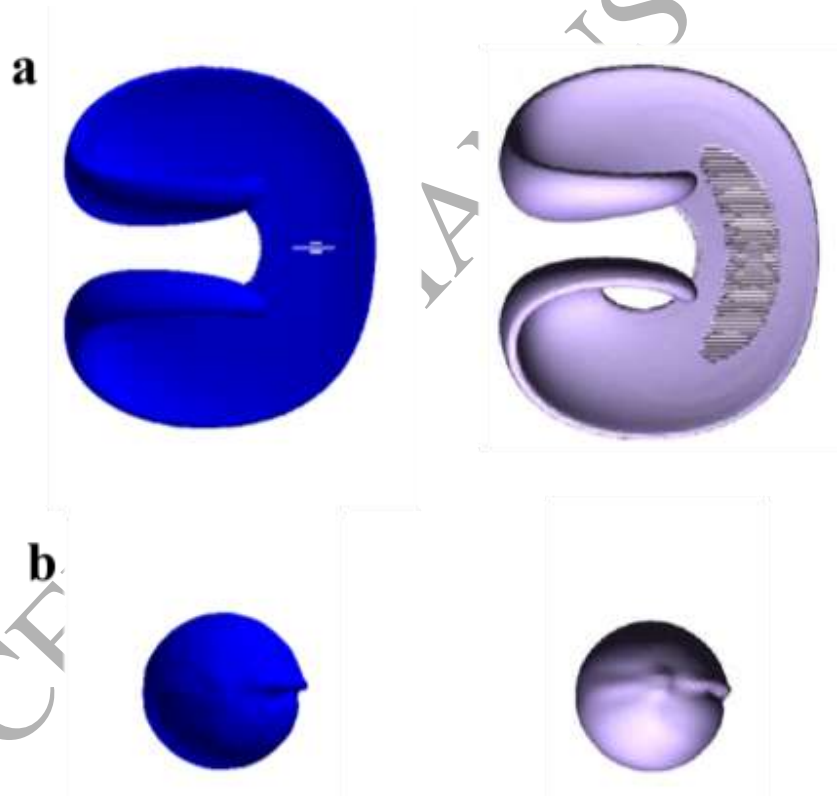

Fig. 3. Deformation of a sphere. (a) t = 1.5, (b) t = 3.0.
Left: present CLSVOF method, right: CLSVOF method of Wang et al. (2009)

To demonstrate the present interface capturing method in overset grid system, the case is also performed in two different overset grid systems. The overset grid system is generated by

embedding some extra grids in the existing uniform Cartesian grid of 150 × 150 × 150. The overset grid system A, shown in Fig. 4(a), is constructed with one slender Cartesian grid of 30 × 30 ×150 with the same grid spacing embedded into the uniform Cartesian grid. The overset grid system B is constructed with two overlapping semi-cylindrical grids of 15 × 107 ×150 embedded into the uniform Cartesian grid, shown in Fig. 4(b). Fig. 5 shows that the interface shapes on these two overset grid systems are very similar to the patterns on the single Cartesian grid in Fig. 3. However, due to the grid interpolation error on the overset grid system, it resulted in somewhat large interface deformation. Table 1 shows the relative mass error and geometry error for each case. It is noted that both the relative mass error and the relative geometry error on overset grid systems are somewhat larger than the measurements on the single Cartesian grid. In addition, there are 27,784 fringe points in the overset grid system A and 103,284 fringe points in the overset grid system B. The overset grid system B introduces more interpolation error than the overset grid system A. Thus, the geometry error in the overset grid system B is much greater than that in the overset grid system A.

Moreover, we also perform the mesh convergence test on both overset grid systems. The dimensions of background uniform Cartesian grid are chosen as 75×75×75, 100×100×100 and 150×150×150 with the increasing finer grid resolution. The dimensions of the embedding inner grids in overset grid system A and B are also adjusted based on the corresponding grid spacing. Table 2 shows the relative mass error and geometry error for the mesh convergence test on overset grid system A and B.

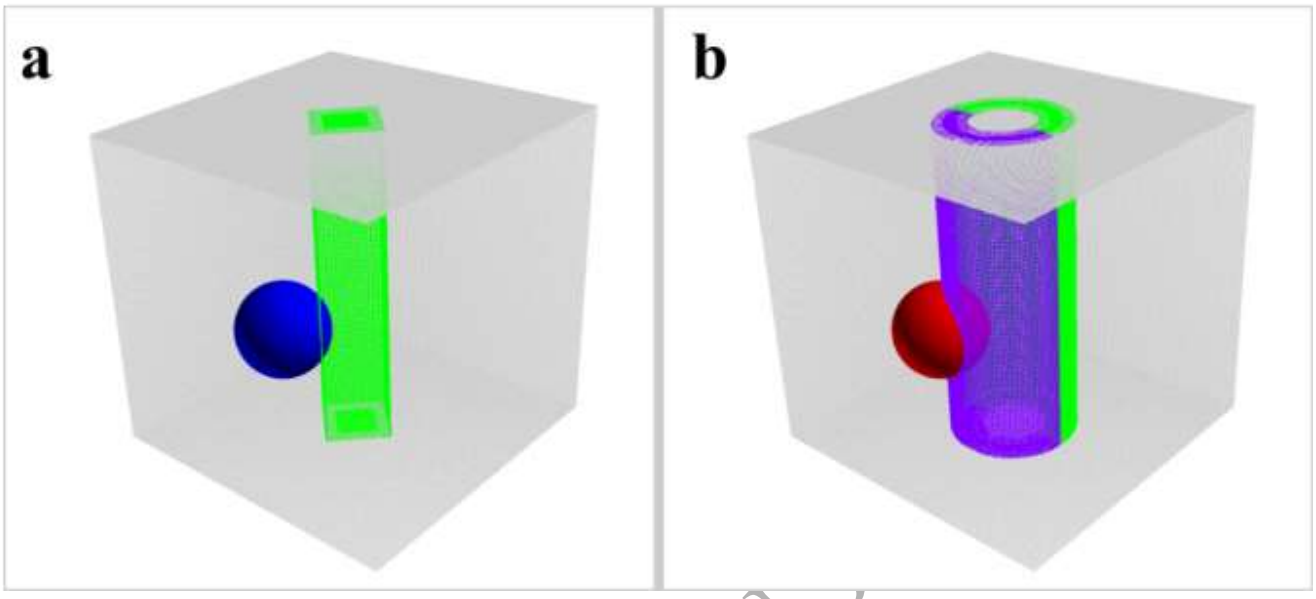

Fig. 4. Overset grid systems for simulation of sphere deformation. (a) Overset grid system A, (b) overset grid system B.

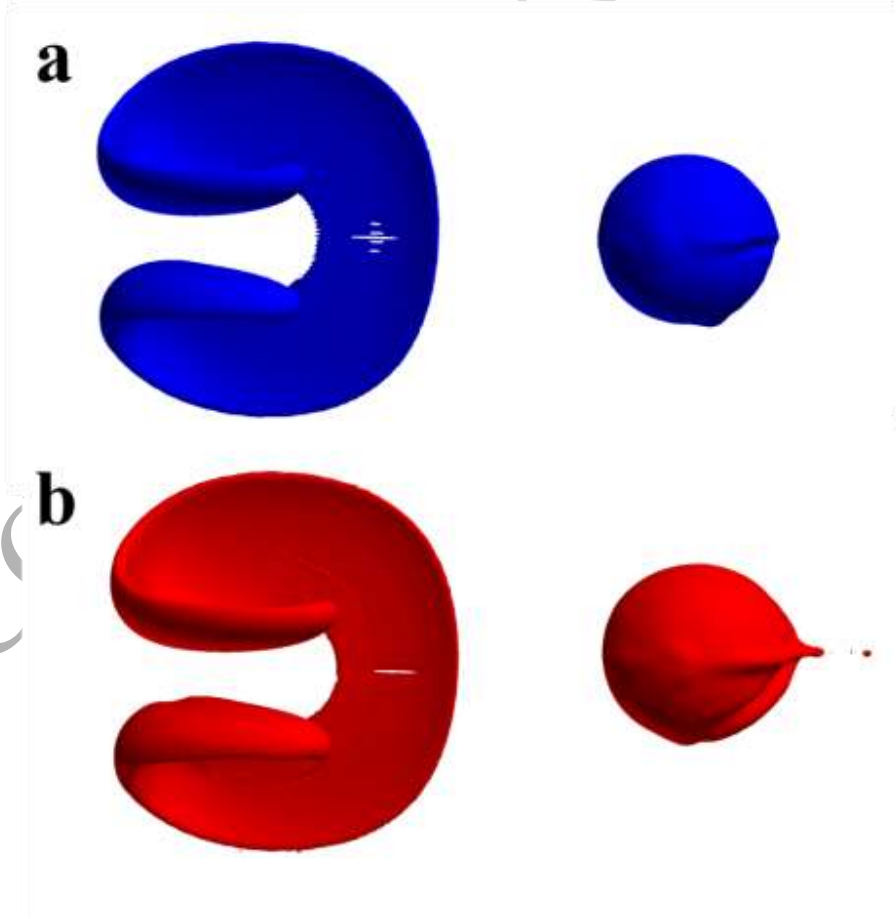

Fig. 5. Deformation of a sphere on an overset grid system. (a) Overset grid system A, (b) Overset grid system B.

Grid	Relative Mass Error (%)	Relative Geometry Error (%)
Uniform Cartesian Grid	1.32×10^{-5}	3.41
Overset Grid System A	0.99×10^{-5}	5.07
Overset Grid System B	1.18×10^{-4}	12.16

Table 1
Relative errors of a deformed sphere in different grids after one period

Over set grid system	Dimension of background grid	Relative Mass Error (%)	Relative Geometry Error (%)
A	75×75×75	1.03×10^{-3}	12.92
A	100×100×100	5.48×10^{-4}	8.57
A	150×150×150	0.99×10^{-5}	5.07
B	75×75×75	7.52×10^{-4}	27.82
B	100×100×100	1.69×10^{-4}	17.15
B	150×150×150	1.18×10^{-4}	12.16

Table 2
Relative errors of a deformed sphere on different overset grid systems after one period

5. Results and discussion

5.1 Dam-breaking flow interacting with a tall square structure

The collapse of a water column over a rigid horizontal plane is called a dam-breaking problem. The classical dam-breaking case is about the collapse of a water column in a tank without any obstacle. This example involves 3D dam-breaking flow interacting with a 3D obstacle. The experimental data was produced by Yeh and Petroff [47]. The tank is 1.6 m long, 0.61 m wide, and 0.75 m high. The square structure, with the size of 0.12 m × 0.12 m × 0.75 m,

is located 0.9 m from upstream of the tank and 0.24 m from the near sidewall of the tank. The volume of 0.4 m × 0.61 m × 0.3 m water is initialized on the upstream of the tank. The numerical tank is utilizing an overset grid system of five multiple Cartesian grids, shown in Fig. 6. The overall domain is represented by one grid. The other four grids assemble the near-field region and each grid occupies one vertical surface of the square structure. Two overset grid systems with different grid points are used in this study: overset grid system A with 831,592 grid points and overset grid system B with 1,772,472 grid points. The characteristic length L = 1 m, characteristic velocity $U_0 = \sqrt{10}\ m/s$ and characteristic time $T_0 = L/U_0$. The overset grid system A used dimensionless grid spacing of 0.01 along all the three axis. The overset grid system B used dimensionless grid spacing of 0.01 in the vertical axis and 0.005 in the horizontal axis. For overset grid system B, much grid refinement is carried out along the tank longitudinal direction. The time increment is 0.001s for both of the overset grid systems. It was assumed that the zero level-set contour was the contact line on a wall.

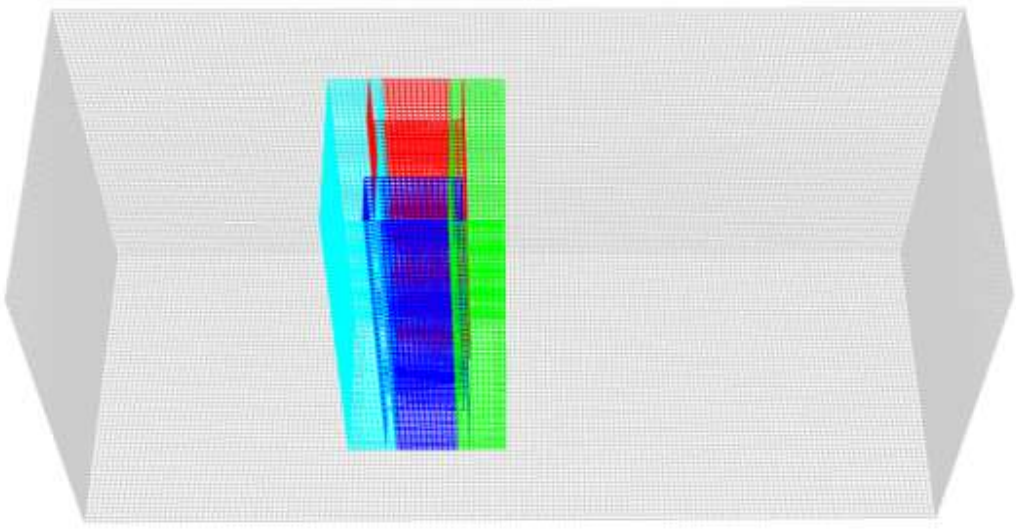

Fig. 6. Overset grid system in the case of dam-breaking flow interacting with a square structure

A series of snapshots of the free surface profiles at different time instants are shown in Fig. 7 to illustrate the complex 3D dam-breaking flow and its interaction with the square structure, as well as the tank sidewalls. At the beginning, the water column collapses quickly by the influence of gravity and flushes to the tank downstream. Once the flow reaches the structure, the middle portion of the flow climbs up the upstream face of the structure. At the same time, both sides of the flow pass the structure and rejoin in the wake of the structure. The converged water continues to move downstream and splashes the downstream tank wall. The splash up of the water also results in the overturning wave with a variety of air pockets in the water. The simulations by Raad and Bidoae by using the Eulerian-Lagrangian marker and micro cell (ELMMC) method [48] are also presented in Fig.7 for comparison.

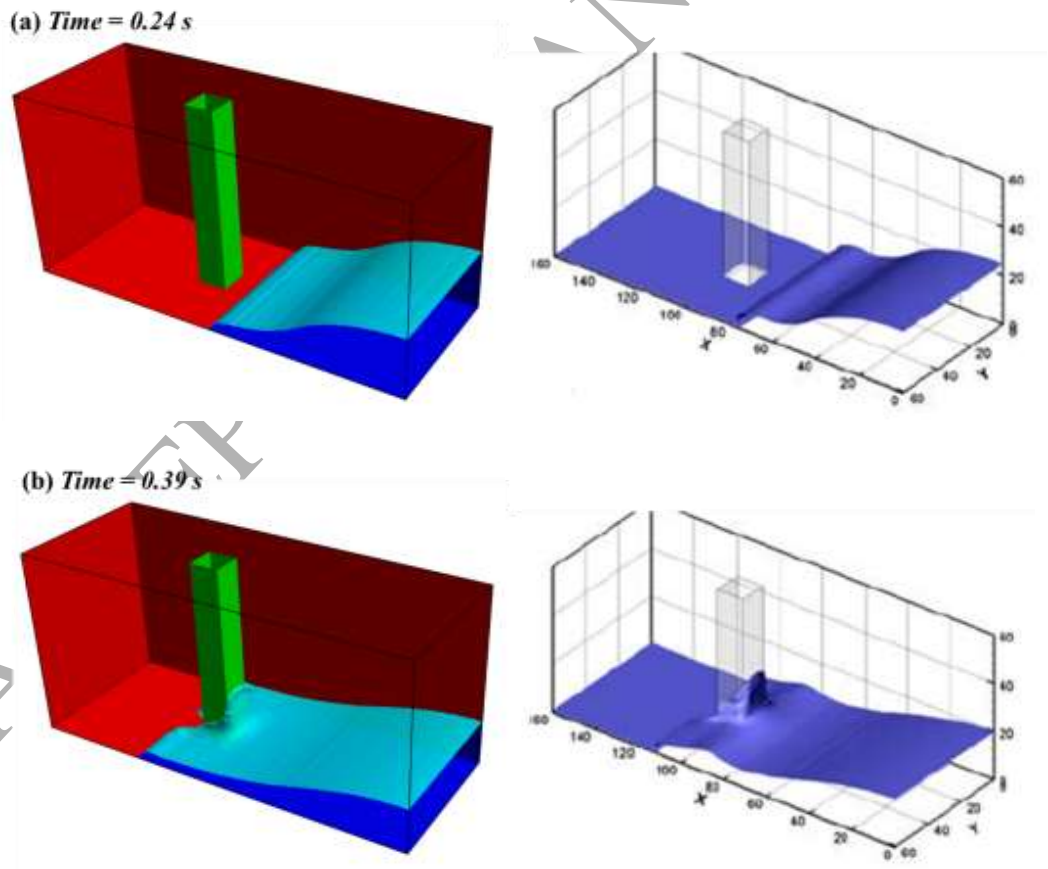

(c) *Time = 0.51 s*

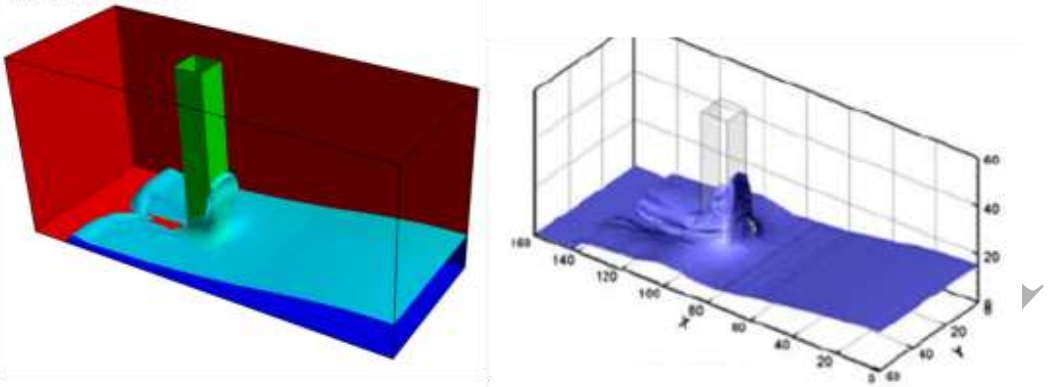

(d) *Time = 0.629 s*

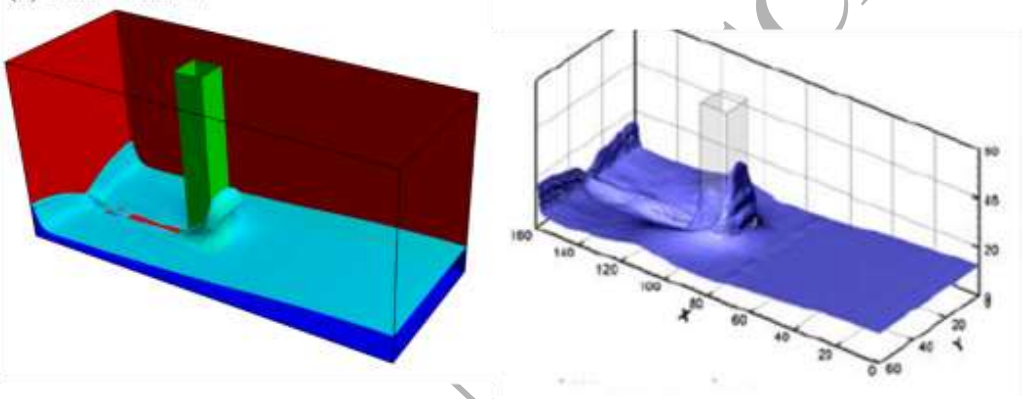

(e) *Time = 0.989 s*

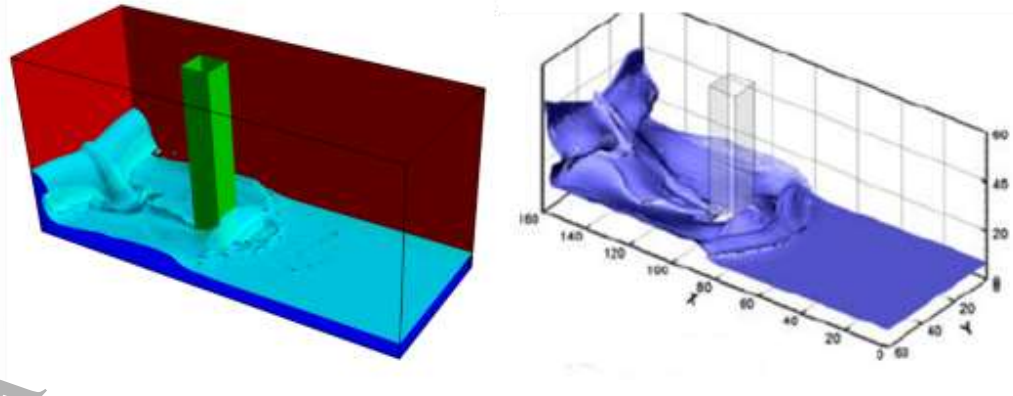

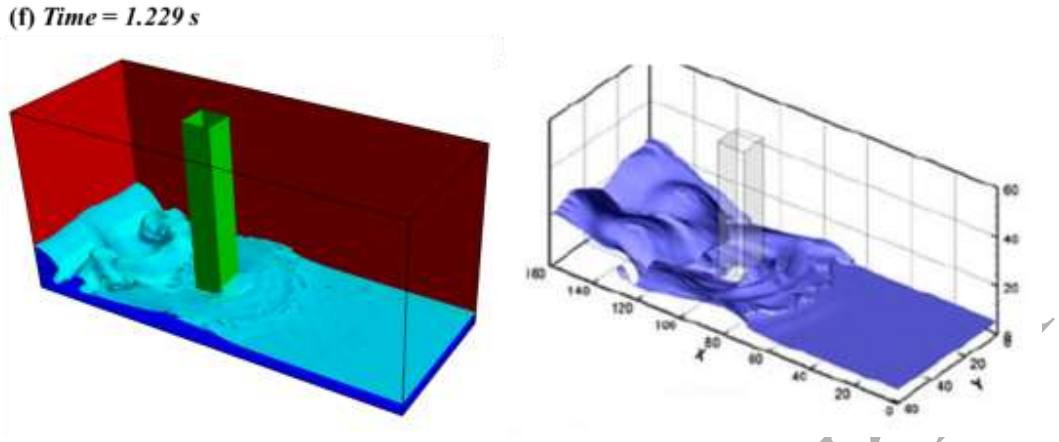

Fig. 7. Snapshots of the dam-breaking flow interacting with the square structure.
Left: present CLSVOF method, right: ELMMC method of Raad and Bidoae (2005)

The net forces on the square structure during the numerical simulation on overset grid system A and B are measured and compared with the experimental data by Yeh and Petroff in Fig. 8. In numerical results, the longitudinal force on structure is calculated by summing the forces acting on the front and back faces of the structure. The force on each boundary cell is calculated by integration of the pressure and the cell area. It can be observed that the predicted impacting force time history is in good agreement with that measured by the experiment. The first impact peak occurs at the time when the flow climbs up the upstream face of the structure. The second impact peak happens at the time when the overturning flow returns to upstream and impacts the downstream of the structure. It is necessary to use fine grid (overset grid system B) for this study to predict the more accurate impacting force peaks.

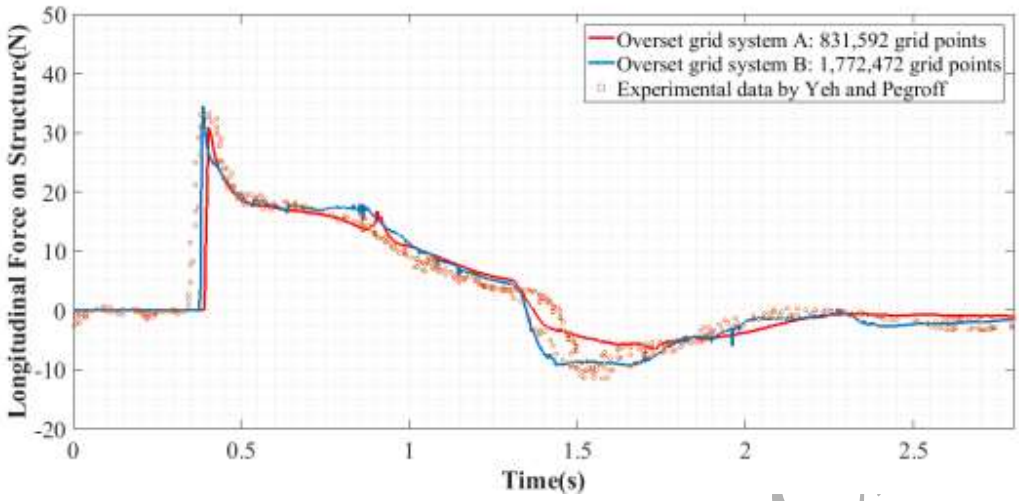

Fig. 8. Time history of the net force on the square structure

5.2 Dam-breaking flow interacting with a circular cylinder

For further study of the dam-breaking flow with obstacle other than square structure, we test the numerical case of dam-breaking flow interacting with a circular cylinder. The case follows the same numerical setup by Lv et al. [49]: the tank is 16 m long, 5 m wide, and 7 m high. A circular cylinder of radius 1 m and height 7 m is placed in the middle of the tank. The still water column is initialized as 4 m long, 5 m wide, and 4.5 m high. The simulation is carried out over the entire tank with an overset grid system. The Fig. 9 shows that the overset grid system is two overlapping semi-cylindrical grids embedded in a Cartesian background grid with 697,007 grid points. The characteristic length L = 1 m, characteristic velocity $U_0 = \sqrt{10}\ m/s$ and characteristic time $T_0 = L/U_0$. The Cartesian background grid used the dimensionless grid spacing of 0.1 along all three axis. The dimensionless mesh size in the cylindrical grids is 0.1 in the polar and longitudinal axis and the polar angle is about 2.57°. Fig. 10 shows that the simulation successfully resolved the wave run-up in front of the pillar, the overturning wave on

the tank wall, and the presence of air pockets behind the cylindrical pillar. The simulation results by Lv et al. using another CLSVOF method on 3D tetrahedral grid are also presented in Fig. 10. It is noted that our numerical results and Lv's results are not at the exact same time instant because Lv didn't indicate the time instant in their works. But it can be seen that the flow patterns in these time instants are very similar. Fig. 11 shows the time history of the relative mass change by our CLSVOF method and the Lv's CLSVOF method. It is clearly seen that our CLSVOF method is capable of good mass conservation to a large extent by using relatively coarse grid.

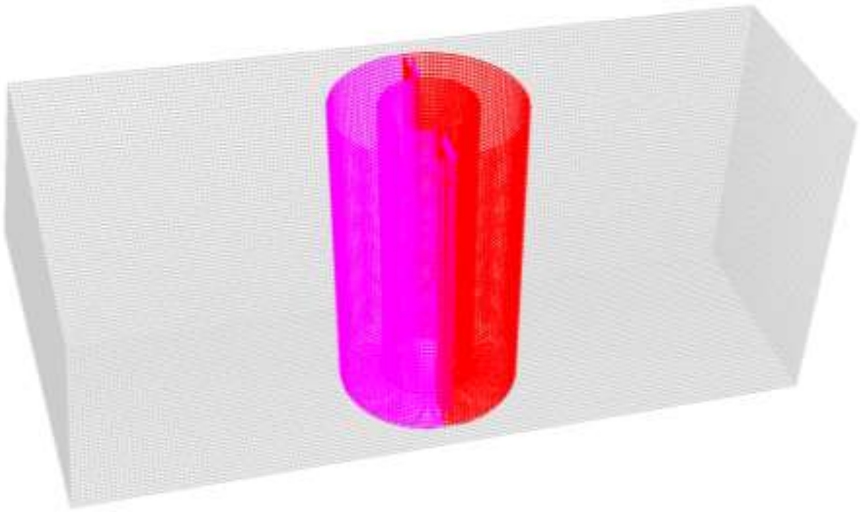

Fig. 9. Overset grid system in the case of dam-breaking flow interacting with a circular cylinder

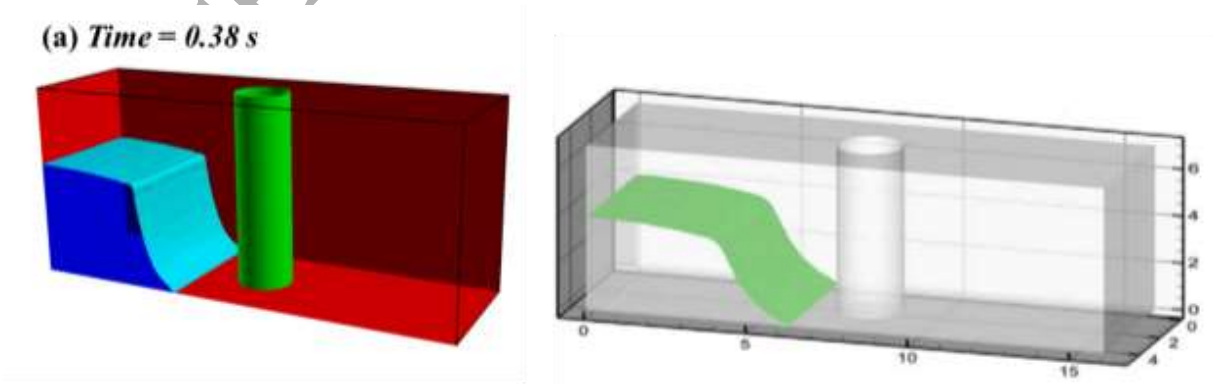

(b) *Time = 0.76 s*

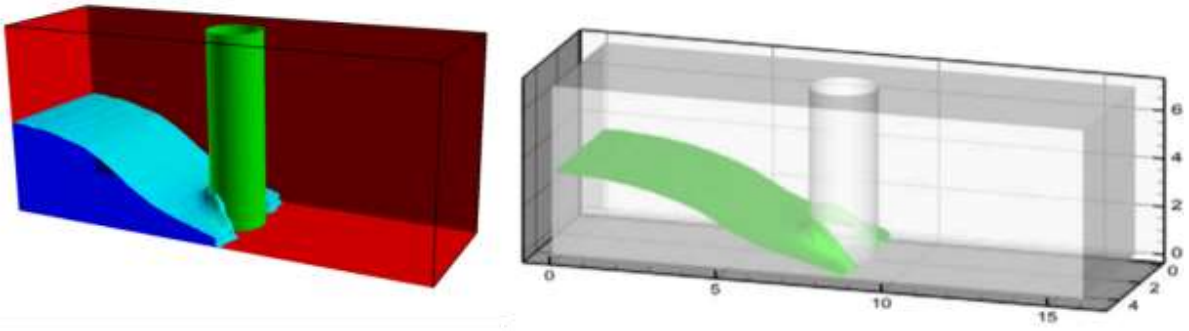

(c) *Time = 1.14 s*

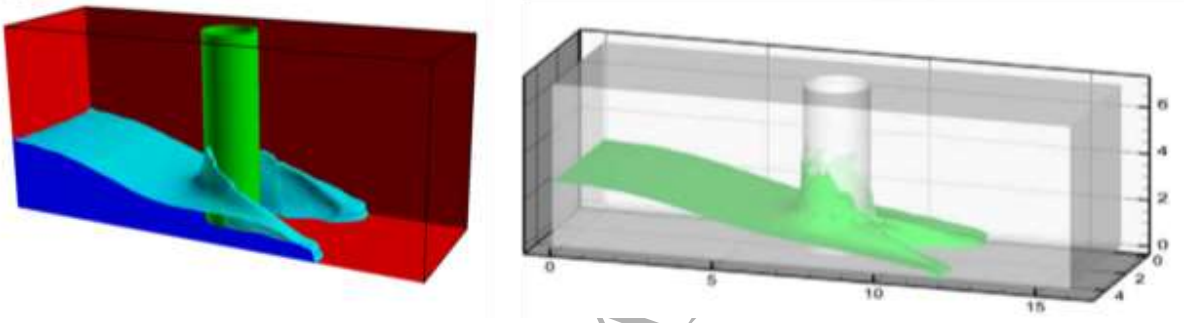

(d) *Time = 1.64 s*

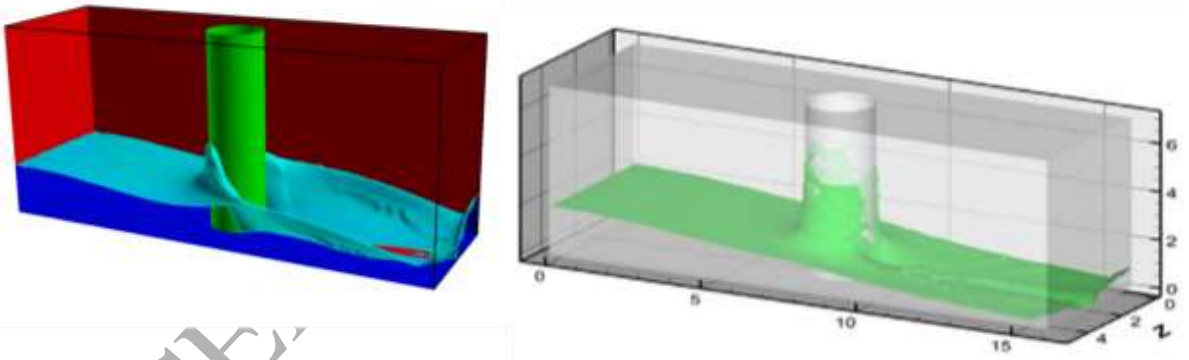

(e) *Time = 2.40 s*

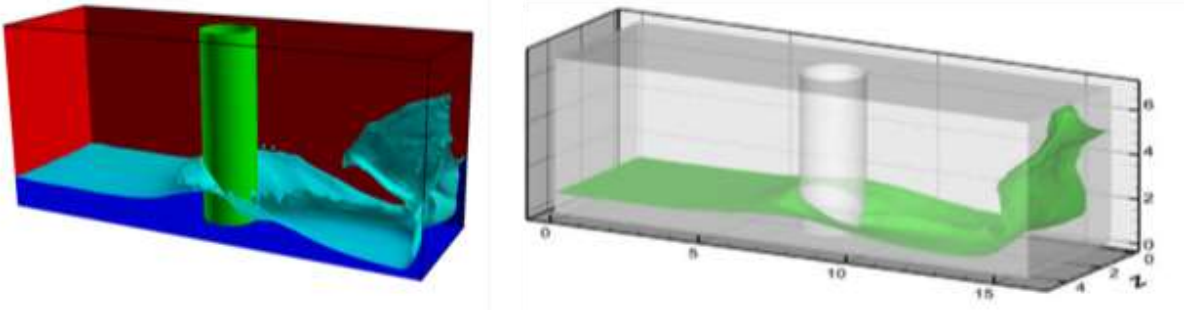

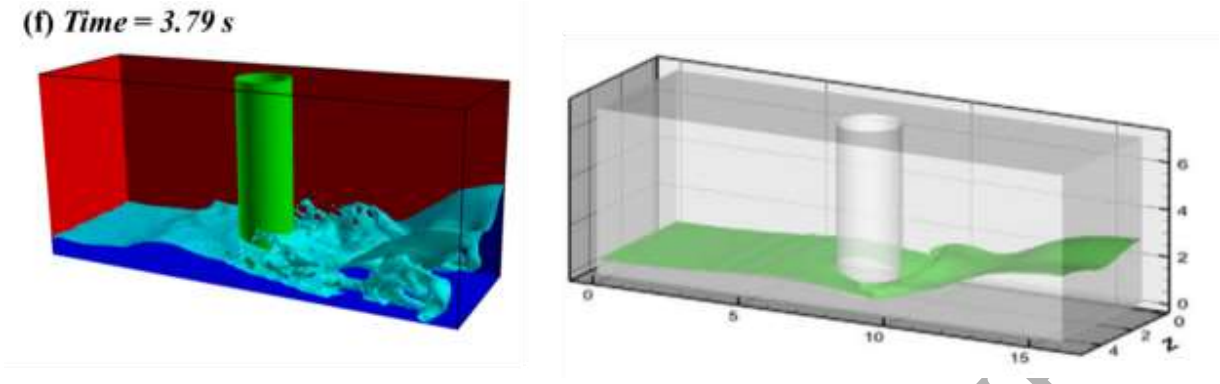

Fig. 10. Snapshots of the dam-breaking flow interacting with the cylinder.
Left: present CLSVOF method, right: CLSVOF method of Lv et al. (2010)

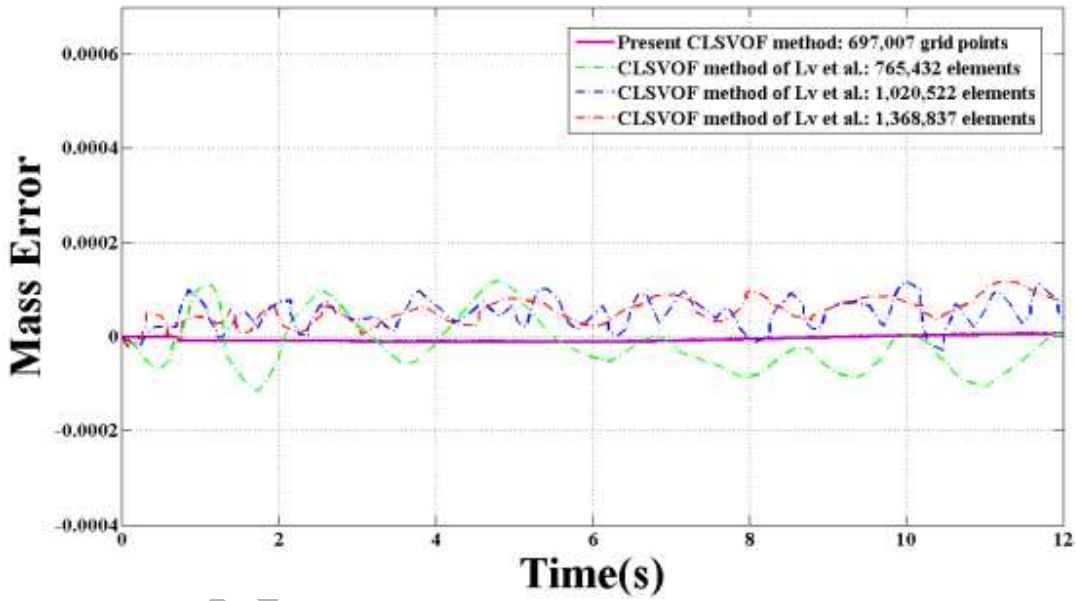

Fig. 11. Time history of the relative mass error.

5.3 Water impact of a hemisphere

In this case, we present the numerical results for water impact of a hemisphere. A hemisphere is moving vertically downward to a water basin with a prescribed speed U_0 of 3.16 m/s. The overset grid system consists of six grid blocks with a total of 493,517 grid points in Fig. 12. The diameter of the sphere is 1.0 m and the water basin is 4 m × 4 m × 10 m. The near-field

boundary-fitted grid blocks are embedded in the Cartesian water basin grid and allowed to move with the hemisphere without tedious grid regeneration. Fig. 13 shows the time-domain simulation results about the water entry of a hemisphere. At the beginning of the impact, the water rises up and at the body sides (Fig. 13(a)). The elevation of the water is increasing as the hemisphere moves to deep water (Fig. 13(b), (c)). To some extent, some water begins to submerge the topside of the hemisphere (Fig. 13(d), (e)). After that, an open cavity is formed on the top of the hemisphere and the open cavity expands laterally (Fig. 13(f), (g)). It is clearly seen that it is much more flexible and efficient to deal with the free surface flow problem involving relative motions by using the present CLSVOF method.

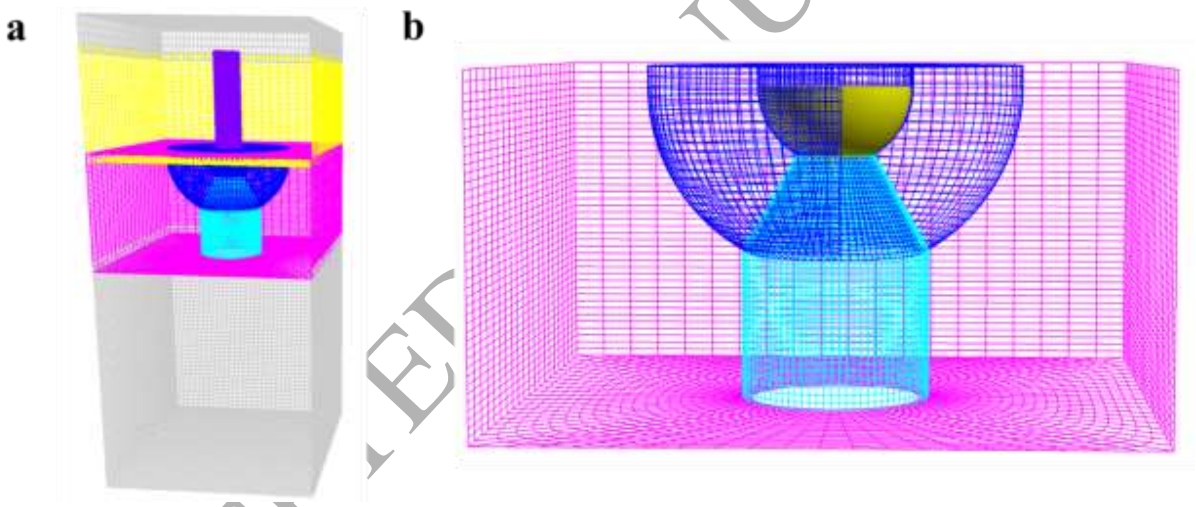

Fig. 12. Overset grid system in the case of water impact of a sphere. (a) Global view, (b) partial view of near-field region.

(a) *Time = 0.16 s*

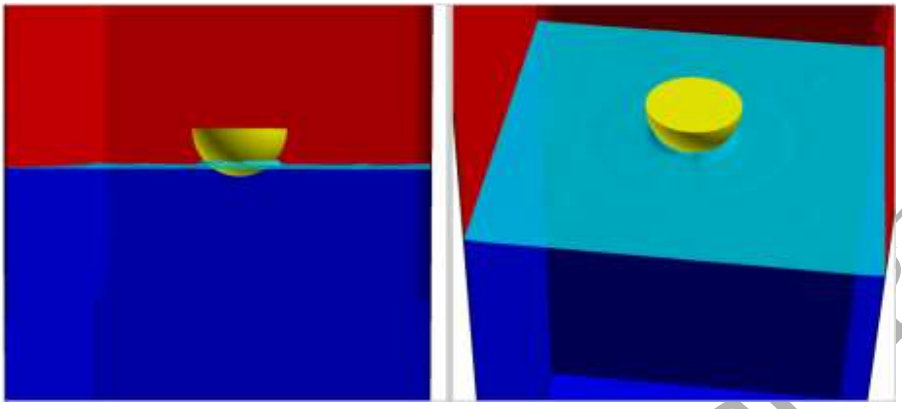

(b) *Time = 0.3 s*

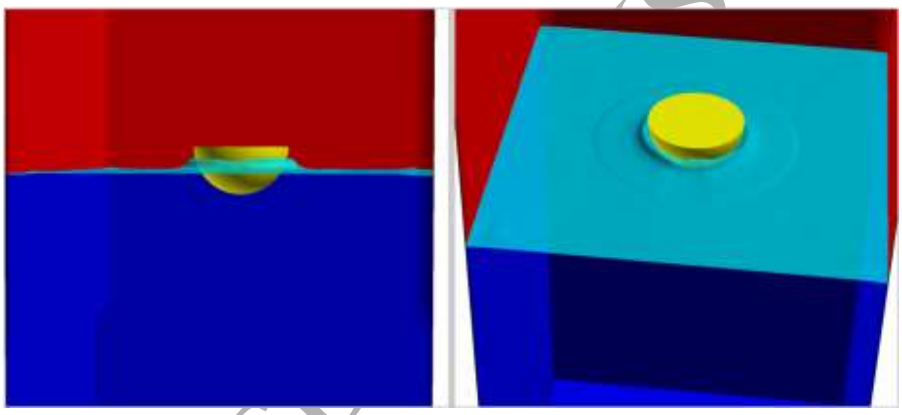

(c) *Time = 0.46 s*

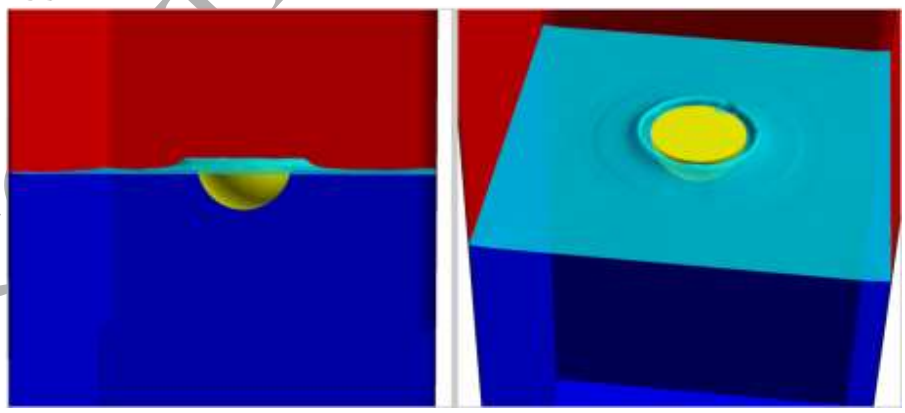

(d) *Time = 0.7 s*

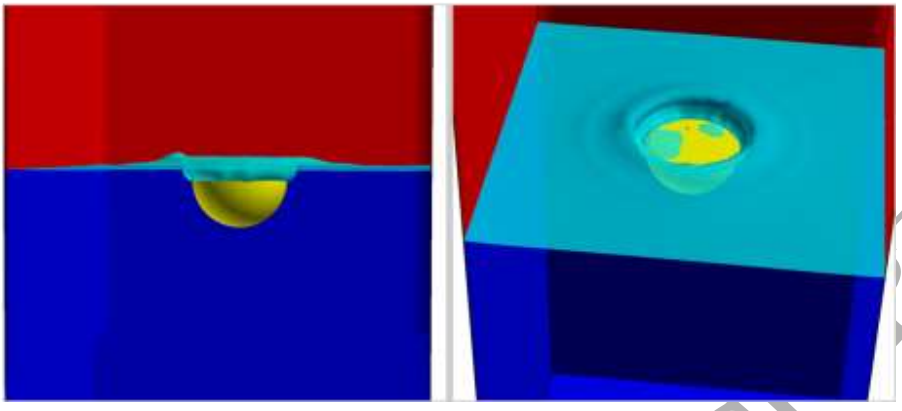

(e) *Time = 0.9 s*

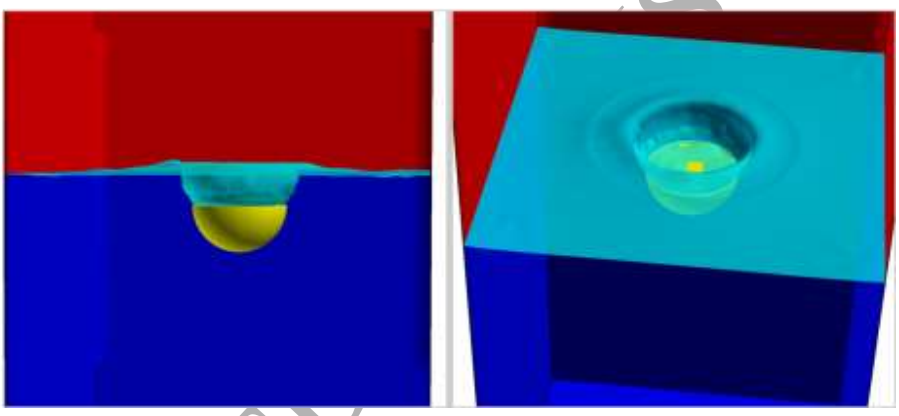

(f) *Time = 1.16 s*

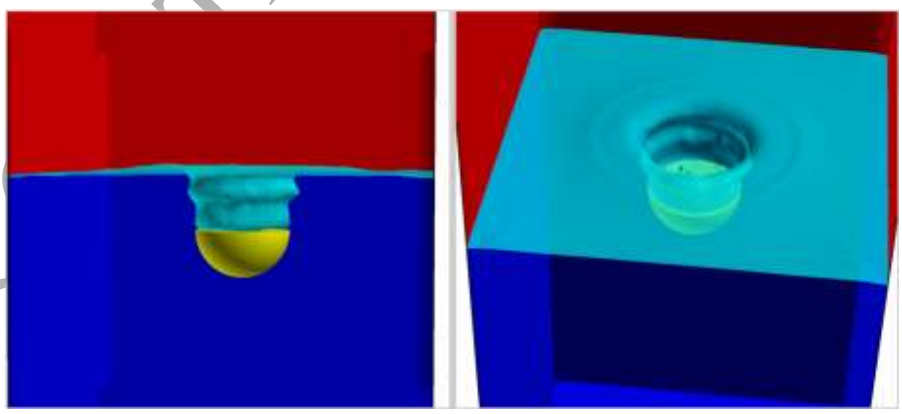

(g) *Time = 1.36 s*

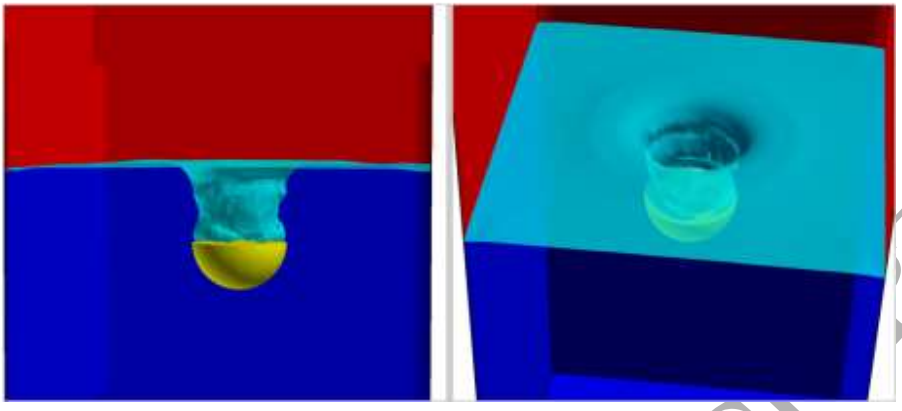

Fig. 13. Snapshots of the water impact of a hemisphere. Left: side view, right: top view

6. Conclusions

In this paper, we presented a new coupled level set and volume-of-fluid method to capture free surface. The novelty of the present method lies in that we developed the CLSVOF method on an overset grid system. The advection test case about stretching of a liquid sphere has been performed to demonstrate the 3D interface capturing ability on several sorts of overset grid system. The results indicated that the present algorithm possesses the ability of high mass conservation and surface capturing. The present method was also validated by the simulation of the dam-breaking flow interacting with structure. The evolution of free surface profiles agreed with some other researchers' numerical results. The net force on structure was in good agreement with the experimental data as well. Another case of hemisphere impacting water was presented by using a moving overset grid system. This case shows that it is much flexible and efficient to deal with the free flow problem involving relative motion by using the present method.

Acknowledgement

The computational resources were provided by the Supercomputing Facility at Texas A&M University (http://sc.tamu.edu).

References

[1] F.H. Harlow, J.E. Welch, Numerical calculation of time-dependent viscous incompressible flow of fluid with a free surface, Phys. Fluids 8 (1965) 2182–2189.

[2] C.W. Hirt, B.D. Nichols, Volume of fluid (VOF) method for the dynamics of free boundaries, J. Comput. Phys. 39 (1981) 201-225.

[3] S.J. Osher, J.A. Sethian, Fronts propagating with curvature dependent speed: algorithms based on Hamilton-Jacobi formulations, J. Comput. Phys. 79 (1988) 12-49.

[4] J.A. Sethian, P. Smereka, Level set methods for fluid interfaces, Annu. Rev. Fluid Mech. 35 (2003) 341–372.

[5] S.O. Unverdi, G. Tryggvason, A front-tracking method for viscous, incompressible, multi-fluid flows, J. Comput. Phys. 100 (1992) 25-37.

[6] W.F. Noh, P.R. Woodward, SLIC (simple line interface method), Lecture Notes in Physics 59 (1976) 330-340.

[7] D.L. Youngs, Time-dependent multi-material flow with large fluid distortion, Numerical Methods for Fluid Dynamics 24 (1982) 273-285.

[8] W.J. Rider, D.B. Kothe, Reconstructing volume tracking, J. Comput. Phys. 141 (1998) 112-152.

[9] D.J.E. Harvie, D.F. Fletcher, A new volume of fluid advection algorithm: the stream scheme, J. Comput. Phys. 162 (2000) 1-32.

[10] R. Scardovelli, S. Zalesaki, Interface reconstruction with least-square fit and split Eulerian-Lagrangian advection, International Journal for Numerical Methods in Fluids 41(2003) 251-274.

[11] J.E. Pilliod, E.G. Puckett, Second-order accurate volume-of-fluid algorithm for tracking material interfaces, J. Comput. Phys. 199 (2004) 465-502.

[12] S. Cummins, M. Francois, D. Kothe, Estimating curvature from volume fractions, Comput. Struct. 83 (2005) 425-434.

[13] S. Popinet, An accurate adaptive solver for surface-tension-driven interfacial flows, J. Comput. Phys. 228 (2009) 5838-5866.

[14] K.M.T. Kleefsman, G. Fekken, A.E.P. Veldman, B. Iwanowski, B. Buchner, A Volume-of-Fluid based simulation method for wave impact problems, J. Comput. Phys. 206 (2005) 363-393.

[15] R.R. Nourgaliev, S. Wiri, N.T. Dinh, T.G. Theofanous, On improving mass conservation of level set by reducing spatial discretization errors, Int. J. Multiphase Flow 31 (2005) 1329–1336.

[16] T.W.H. Sheu, C.H. Yu, P.H. Chiu, Development of a dispersively accurate conservative level set scheme for capturing interface in two-phase flows, J. Comput. Phys. 228 (2009) 661–686.

[17] M. Sussman, P. Smereka, S. Osher, A level set approach for computing solutions to incompressible two-phase flow, J. Comput. Phys. 114 (1994) 146–159.

[18] M. Sussman, E. Fatemi, P. Smereka, S. Osher, An improved level set method for incompressible two-phase flows, J. Comput. Fluids 27 (1998) 663–680.

[19] Y.C. Chang, T.Y. Hou, B. Merriman, S. Osher, A level set formulation of Eulerian interface capturing methods for incompressible fluid flows, J. Comput. Phys. 124 (1996) 449–464.

[20] M. Sussman, E.G. Puckett, A coupled level set and volume-of-fluid method for computing 3D and axisymmetric incompressible two-phase flows, J. Comput. Phys. 162 (2000) 301–337.

[21] M. Sussman, A second order coupled level set and volume-of-fluid method for computing growth and collapse of vapor bubbles, J. Comput. Phys. 187 (2003) 110–136.

[22] G. Son, N. Hur, A coupled level set and volume-of-fluid method for the buoyancy-driven motion of fluid particles, Numer. Heat Transf. B 42 (2002) 523-542.

[23] Z. Wang, J. Yang, B. Koo, F. Stern, A coupled level set and volume-of-fluid method for sharp interface simulation of plunging breaking waves, Int. J. Multiphase Flow 35 (2009) 227-246.

[24] N. Ashgriz, T. Barbat, G. Wang, A computational Lagrangian-Eulerian advection remap for free surface flows, Int. J. Numer. Methods Fluids 44 (2004) 1-32.

[25] X. Yang, A.J. James, J. Lowengrub, X. Zheng, V. Cristini, An adaptive coupled level-set/volume-of-fluid interface capturing method for unstructured triangular grids, J. Comput. Phys. 217 (2006) 364–394.

[26] M. Sussman, A parallelized, adaptive algorithm for multiphase flows in general geometries, J. Comput. Struct. 83 (2005) 435-444.

[27] C.S. Peskin, Flow patterns around heart valves: a numerical method, J. Comput. Phys. 10 (1976) 252–271.

[28] H.C. Chen, K. Yu, CFD simulation of wave-current-body interactions including greenwater and wet deck slamming, Comput. Fluids 38 (2009) 970-980.

[29] G.S. Jiang, C.W. Shu, Efficient implementation of weighted ENO schemes, J. Comput. Phys. 126 (1996) 202-228.

[30] D. Gueyffier, J. Li, A. Nadim, R. Scardovelli, S. Zaleski, Volume-of-Fluid interface tracking with smoothed surface stress methods for three-dimensional flows, J. Comput. Phys. 152 (1999) 423-456.

[31] Y. Zhao, H.C. Chen, Numerical simulation of 3D sloshing flow in partially filled LNG tank using a coupled level-set and volume-of-fluid method, Ocean Eng. 104 (2015) 10-30.

[32] Y. Zhao, H.C. Chen, X. Yu, Numerical simulation of wave slamming on 3D offshore platform deck using a coupled level-set and volume-of-fluid method for overset grid system, Ocean. Syst. Eng. 5 (2015) 245-259.

[33] R.P. Brent, Algorithms for minimization without derivatives, Englewood Cliffs, NJ: Prentice-Hall, (1973).

[34] E. Aulisa, S. Manservisi, R. Scardovelli, S. Zaleski, Interface reconstruction with least-squares fit and split advection in three-dimensional Cartesian geometry, J. Comput. Phys. 225 (2007) 2301-2319.

[35] Y. Zhao, H.C. Chen, CFD simulation of violent free surface flows by a coupled level-set and volume-of-fluid method, In: Proceedings of the Twenty-third (2013) International Offshore and Polar Engineering Conference, Anchorage. 30 June-4 July. USA, 968-975.

[36] Y. Zhao, H.C. Chen, Violent free surface flow simulations by a coupled level-set and volume-of-fluid method in over set grid systems, Int. J. Offshore Polar Eng. 24 (2014) 114–121.

[37] A. Bourlioux, A coupled level-set volume-of-fluid algorithm for tracking material interfaces, In: Proceedings of the sixth (1995) International Symposium on Computational Fluid Dynamics, Lake Tahoe, USA.

[38] G. Son, A coupled level set and volume-of-fluid for the buoyancy-driven motion of fluid particles, Numerical Heat Transfer Part B 42 (2002) 523-542.

[39] G. Son, Efficient implementation of a coupled level-set and volume-of-fluid method for three-dimensional incompressible two-phase flows, Numerical Heat Transfer Part B 43 (2003) 549-565.

[40] T. Menard, S. Tanguy, A. Berlemont, Coupling level set/VOF/ghost fluid methods: Validation and application to 3D simulation of the primary break-up of a liquid jet, Int. J. Multiphase Flow 33 (2007) 510-524.

[41] Z. Wang, J. Yang, F. Stern, A new volume-of-fluid method with a constructed distance function on general structured grids, J. Comput. Phys. 231 (2012) 3703-3722.

[42] Y. Zhao, Numerical simulations of violent free surface by a coupled level-set and volume-of-fluid method, Doctoral dissertation (2014) Texas A&M University.

[43] J. Benek, J. Steger, F.C. Dougherty, A flexible grid embedding technique with application to the Euler equations, 6th computational fluid dynamic conference (1983).

[44] M. Robert, On the spatial and temporal accuracy of overset grid methods for moving body problems, 12th applied aerodynamics conference (1994).

[45] R. LeVeque, High-resolution conservation algorithms for advection in incompressible flow, SIAM J. Numer. Anal. 33 (1996) 627.

[46] D. Enright, R. Fedkiw, J. Ferziger, I. Mitchell, A hybrid particle level set method for improved interface capturing, J. Comput. Phys. 183 (2002) 83-116.

[47] H. Arnason, C. Petrof, H. Yeh, Tsunami bore impingement onto a vertical column, J. Disaster Research 4.6 (2009), 391-403.

[48] P.E. Raad, R. Bidoae, The three-dimensional Eulerian-Lagrangian marker and micro cell method for the simulation of free surface flows, J. Comput. Phys. 203 (2005) 668-699.

[49] X. Lv, Q. Zou, Y. Zhao, D. Reeve, A novel coupled level set and volume of fluid method for sharp interface capturing on 3D tetrahedral grids, J. Comput. Phys. 229 (2010) 2573-2604.